Room temperature microwave oscillations in GaN/AlN resonant tunneling diodes with peak current densities up to 220 kA/cm^2

Jimy Encomendero,[1,a)] Rusen Yan,[1] Amit Verma,[2] S. M. Islam,[1] Vladimir Protasenko,[1] Sergei Rouvimov,[3] Patrick Fay,[3] Debdeep Jena,[1,4,b)] and Huili Grace Xing[1,4,5,c)]
[1]*School of Electrical and Computer Engineering, Cornell University, Ithaca, New York 14853, USA*
[2]*Department of Electrical Engineering, Indian Institute of Technology Kanpur, Kanpur 208016, India*
[3]*Department of Electrical Engineering, University of Notre Dame, Notre Dame, Indiana 46556, USA*
[4]*Department of Materials Science and Engineering, Cornell University, Ithaca, New York 14853, USA*
[5]*Kavli Institute at Cornell for Nanoscale Science, Cornell University, Ithaca, New York 14853, USA*

(Received 19 November 2017; accepted 28 January 2018; published online 5 March 2018)

We report the generation of room temperature microwave oscillations from GaN/AlN resonant tunneling diodes, which exhibit record-high peak current densities. The tunneling heterostructure grown by molecular beam epitaxy on freestanding GaN substrates comprises a thin GaN quantum well embedded between two AlN tunneling barriers. The room temperature current-voltage characteristics exhibit a record-high maximum peak current density of ~220 kA/cm^2. When biased within the negative differential conductance region, microwave oscillations are measured with a fundamental frequency of ~0.94 GHz, generating an output power of ~3.0 μW. Both the fundamental frequency and the output power of the oscillator are limited by the external biasing circuit. Using a small-signal equivalent circuit model, the maximum intrinsic frequency of oscillation for these diodes is predicted to be ~200 GHz. This work represents a significant step towards microwave power generation enabled by resonant tunneling transport, an ultra-fast process that goes beyond the limitations of current III-Nitride high electron mobility transistors. *Published by AIP Publishing.*
https://doi.org/10.1063/1.5016414

Recent years have seen an increasing demand for terahertz (THz) electronic and photonic devices, fueled by the broad range of practical applications enabled by THz waves. To meet these needs, III-Nitride-based high electron mobility transistors (HEMTs) have emerged as potential electronic device candidates due to their high electron velocity, high two-dimensional (2D) electron gas density, and high thermal conductivity.[1–4] However, despite the steady progress in high-frequency performance, III-Nitride HEMTs are yet to achieve amplification at frequencies >1 THz. In this scenario, non-conventional transport mechanisms such as 2D plasma-waves have been proposed as a means to overcome traditional HEMT limitations.[5,6] More recently, THz amplification exceeding 5 dB was predicted when plasma-waves are excited via resonant tunneling injection.[7]

Resonant tunneling transport, being an extremely fast quantum mechanical process, has been extensively studied over the last five decades,[8–20] leading to the demonstration of the fastest THz electronic oscillators reported to date.[21] Over this period, various photonic and electronic devices that exploit this quantum effect were conceived and realized employing different material systems, including arsenides[10,22] and antimonides.[11,23] However, within the III-Nitride family of semiconductors, reproducible high-current resonant tunneling transport has remained elusive at room temperature (RT) until very recently.

Initially, repeatable resonant tunneling signatures were reported at cryogenic temperatures in nanowire III-Nitride heterostructures.[24] However, it has been only during the last five years that repeatable resonant tunneling transport and its characteristic negative differential conductance (NDC) have been reported in III-Nitride tunneling heterostructures at RT.[12–15]

Repeatable NDC at 300 K was initially achieved using a GaN/AlN resonant tunneling superlattice.[12] The device, epitaxially grown on an AlN film deposited on sapphire, comprised seven GaN quantum wells confined by AlN barriers. The multiple-barrier design attenuates any leakage current, thus enabling the measurement of multiple resonances at RT. However, the resonant tunneling current component was also severely attenuated, yielding a peak current density of ~4.2 mA/cm^2 and a peak-to-valley current ratio (PVCR) of ~1.4.

More recently, repeatable NDC was also reported in GaN/Al$_x$Ga$_{1-x}$N double-barrier resonant tunneling diodes (RTDs).[16,17] Peak current densities up to ~375 kA/cm^2 were measured in these devices at cryogenic temperatures due to the lower conduction band discontinuity: $\Delta E_C \approx 0.58$ eV,[17] comparable to that between lattice matched InGaAs and InAlAs. However, the NDC vanished at RT, suggesting that thermally activated leakage paths through dislocations are the dominant conduction mechanism at 300 K.[17]

RTDs featuring AlN barriers have also been recently reported by Growden *et al.*[15] and by us.[13,14] Highly repeatable NDC was observed in these devices at cryogenic and room temperatures. Typical peak current densities up to ~6.4 kA/cm^2 were recorded at RT for RTDs with ~2 nm-barriers—equivalent to 8 monolayers (ML)—and a ~3 nm (12 ML)-wide GaN quantum well.[13,14] The peak tunneling current was further increased up to ~26 kA/cm^2 using

a)Electronic mail: jje64@cornell.edu
b)Electronic mail: djena@cornell.edu
c)Electronic mail: grace.xing@cornell.edu

thinner AlN barriers down to ∼1.5 nm (6 ML). However, theoretical calculations predict even higher current-densities in III-Nitride RTDs when thinner tunneling barriers and narrower quantum wells are employed.[14]

In the present letter, we report III-Nitride RTDs which exhibit record-high peak current densities up to ∼220 kA/cm^2 and demonstrate a RTD microwave oscillator working at room temperature. By precise control over the thickness of the epitaxially grown layers, a thin ∼1.75 nm (7 ML)-wide GaN quantum well was incorporated in the device structure. The generation of self-oscillations at RT attests to the high reliability of the NDC present in these devices. The fundamental oscillation frequency of the RTD oscillator was measured at ∼0.94 GHz, which is shown to be limited by the external biasing circuit. By using a small-signal equivalent circuit model, we found an upper bound on the maximum frequency of oscillation expected from these devices. These results demonstrate that III-Nitride RTDs can be employed as gain elements in high-frequency electronic oscillators. Furthermore, by additional improvements in the device structure and series resistance, oscillation frequencies approaching the THz band are predicted.

The device structure, grown by molecular beam epitaxy (MBE), is schematically shown in the inset of Fig. 1(a). The heterostructure was epitaxially grown on commercially available n-type single-crystal GaN substrates with nominal dislocation densities $<5\times10^4$ cm^{-2}.[25] Metal-rich growth conditions were maintained during the whole epitaxial process to promote the step-flow growth mode and minimize roughness of the epitaxial layers. A substrate temperature of ∼740 °C, as measured using a thermocouple, was kept constant throughout the growth. The nitrogen plasma power was also kept constant at 200 W, thus achieving a growth rate of ∼2.1 nm/min.

The device structure comprises two ∼100 nm-thick n-GaN layers, degenerately doped with silicon donors. These

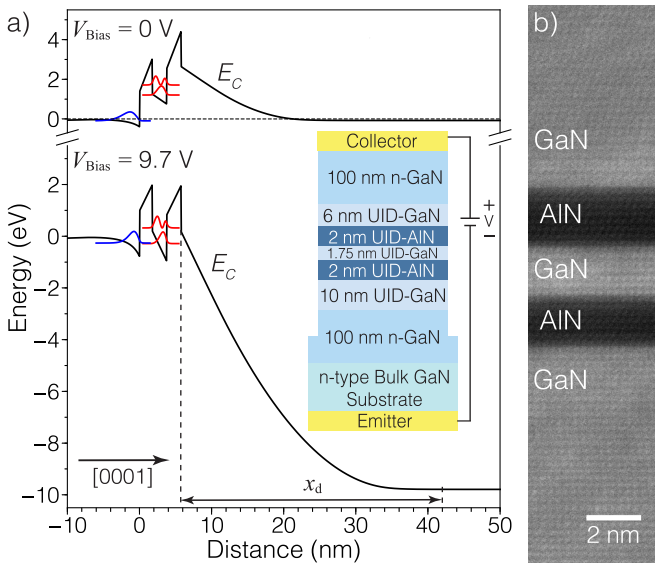

FIG. 1. (a) Band diagram of the device structure at equilibrium (top panel) and under resonant bias (lower panel). The inset shows the schematic cross-section of a device under forward bias. (b) High angle annular dark-field (HAADF) scanning transmission electron microscopy (STEM) image of the GaN/AlN double barrier heterostructure.

layers, which act as contact electrodes, were doped with a nominal concentration of $\sim1\times10^{19}$ cm^{-3} as depicted in the inset of Fig. 1(a). Un-intentionally doped (UID) spacers were also introduced next to the contact layers to minimize dopant diffusion into the active region. Moreover, asymmetric spacers were employed to reduce the extension of the collector depletion region next to the top contact layer [See the top panel of Fig. 1(a)]. Thus, the device features a 10 nm-thick emitter spacer, whereas a thinner 6 nm-UID GaN layer acts as the collector spacer. The active region comprises two AlN barriers with a nominal thickness of ∼2 nm (8 ML), confining the resonant states of a ∼1.75 nm (7 ML)-wide GaN quantum well.

Post-growth characterization was performed using high angle annular dark-field (HAADF) scanning transmission microscopy (STEM). A HAADF STEM image of the active region shows abrupt transitions between the AlN tunneling layers and the GaN quantum well [Fig. 1(b)]. Even though the device structure was designed to have symmetric barriers, some asymmetry between the collector and emitter barriers can be seen in Fig. 1(b).

The effects of asymmetric barriers were studied early on after the first RTDs were fabricated.[26] Ricco *et al.* showed that electron waves experience un-attenuated transmission only when the single-barrier transmission coefficient is the same for both barriers. This condition is readily satisfied at zero bias in the case of non-polar RTDs. However in the polar case, the situation is the opposite: at zero bias conditions [see Fig. 1(a), top panel], the conduction band energy profile E_C is highly asymmetric, resulting in an attenuated global transmission coefficient ($T<1$). However, under forward bias, a symmetric configuration can be still attained in polar RTDs. This situation occurs roughly close to resonant conditions as shown in the bottom panel of Fig. 1(a). Under these conditions, the energy profile of each of the barriers becomes equivalent, which leads to symmetric single-barrier transmission coefficients and, as a result, $T\approx1$. It should be noted however that due to the strong internal electric fields within the barriers, this unity transmission can be obtained only when both barriers have the same thickness. As a consequence, any fluctuations which break the symmetry of the structure will lead to significant variations in the resonant tunneling current. Using an analytical model for polar RTDs, we will quantify these effects and compare them with our experimental results.

RTDs were fabricated using contact lithography, reactive ion etching, and metal evaporation. Arrays of mesas of $\sim5\times5$ μm^2 were defined employing a self-aligned process. A second metalization step was employed to define the emitter contact on the back of the substrate, obtaining the device structure depicted in the inset of Fig. 1(a).

Transfer length method (TLM) structures were also defined to obtain the contact resistance present at the metal-semiconductor interface. From the collector TLM structure, a specific contact resistance of ∼100 Ω μm^2 was obtained. Thus, when a device is biased at a maximum peak current density of 200 kA/cm^2, a maximum voltage drop of ∼200 mV would be expected at the collector contact. This contact voltage drop shifts the resonant voltage slightly while also increasing the DC power dissipation; in this sense,

minimizing its impact would be paramount in high-performance III-Nitride RTDs.

The energy band diagram of the heterostructure was calculated using a self-consistent Schrödinger-Poisson solver.[27] The top panel of Fig. 1(a) shows the conduction band energy profile E_C, at equilibrium. As a result of the strong polarization fields, free carriers redistribute across the active region while the bottom of the quantum well rises ∼1 eV above the Fermi level. This polarization-induced asymmetric conduction band profile is characteristic of polar RTDs and results from the broken inversion symmetry of the crystal which generates the spontaneous and piezoelectric polarization fields.[14]

A direct consequence of the polarization fields is that resonant tunneling conditions are typically achieved only under forward bias.[14] To estimate the expected resonant voltage, the subband energy levels of the quantum well were calculated employing the envelope function approximation.[28] Due to the strong confinement introduced by the AlN barriers, non-parabolicity effects within the well are also considered by means of an energy-dependent effective mass dispersion, calculated from an 8-band $\vec{\mathbf{k}} \cdot \vec{\mathbf{p}}$ model.[29] As shown in the bottom panel of Fig. 1(a), resonant conditions are achieved at ∼9.7 V when the ground-state in the quantum well aligns with the emitter bound-state located within the accumulation region. This result is consistent with the experimental measurements, to be discussed in the remainder of this letter.

Current-voltage (*I-V*) characteristics are measured at RT using a semiconductor parameter analyzer. Sixty-two devices with mesa areas of $\sim 5 \times 5\ \mu m^2$ were tested under forward bias. Typical peak current densities (J_p) between 140 and 180 kA/cm^2 were obtained across the $\sim 5 \times 5$ mm^2 chip. Figure 2(a) summarizes the distribution of the peak currents, which range from a minimum value of ∼103 kA/cm^2 up to a maximum of ∼220 kA/cm^2.

The distribution of peak current might be due to random fluctuations in the barrier thickness. To quantify this effect, we calculate the expected resonant tunneling current using an analytical model for polar RTDs,[14] keeping the GaN well thickness fixed at 1.75 nm (7 ML). For the symmetric case in which both barriers are 2 nm (8 ML)-thick, a $J_p \approx 140$ kA/cm^2 is expected. Meanwhile, for single ML variations in the emitter barrier, we found $J_p \approx 200$ kA/cm^2 for a 7-ML emitter barrier and $J_p \approx 70$ kA/cm^2 for a 9-ML emitter barrier. The consequences of single ML fluctuations in the collector barrier can also be calculated: we obtained $J_p \approx 180$ kA/cm^2 and $J_p \approx 80$ kA/cm^2 for a 7-ML and 9-ML collector barrier, respectively. This spread is consistent with the experimental data shown in Fig. 2(a).

Figure 2(b) displays the distribution of the PVCR for the same set of devices, which exhibit a typical PVCR between 1.1 and 1.15. Moreover, PVCRs as high as ∼1.34 were recorded from two different devices. It should be noted however that RTDs with the highest peak current densities (∼220 kA/cm^2) presented PVCRs of the order of ∼1.05. This trend of decreasing PVCR in high-current density RTDs has been previously reported in other material systems.[19,20] This negative correlation stems from the enhancement of scattering events in the quantum well as a result of a larger electron subband population.[20] Furthermore, the higher power dissipation (and thus temperature) also plays a role, smearing the Fermi distribution, thereby enhancing thermionic emission. Consequently, devices operating at lower biases are expected to provide larger PVCRs as discussed below.

The set of devices under study present peak voltages V_p distributed between 8.0 and 10.4 V as shown in Fig. 2(c). Meanwhile, the valley voltage (V_v) values exhibit a range that extends from 8.4 V up to 11.2 V [See Fig. 2(d)]. It should be noted however that more than a third of the RTDs exhibit a $V_p \approx 9.2$ V as can be seen from the distribution displayed in Fig. 2(c). This result is consistent with our theoretical prediction of ∼9.7 V.

The room temperature *I-V* characteristics of a forward biased RTD are presented in Fig. 2(e). The peak current density of this particular device is measured at ∼180 kA/cm^2 with a valley current of ∼135 kA/cm^2, providing a PVCR of ∼1.34. Under reverse bias, no resonant peak is observed; instead, the current increases monotonically as shown in the plot of Fig. 2(f). This asymmetric *I-V*, characteristic of polar RTDs, is a direct consequence of the internal spontaneous and piezoelectric polarization fields.[14]

The chair-like behavior measured within the NDC region results from self-oscillations generated by the unstable circuit.[30–32] These oscillations build up as a result of the dynamic negative conductance that counteracts any lossy elements in the resonant circuit.

Tunneling transport being an extremely fast process, with characteristic time $\tau < 1$ ps, has been employed as the gain mechanism in various microwave,[30] millimeter-wave,[33–36] and THz[21,37] electronic oscillators. In this work, we demonstrate a microwave oscillator driven by a GaN/AlN RTD operating at RT.

The oscillator circuit is composed of the RTD connected through an on-wafer probe, coaxial cables, and a bias tee to a

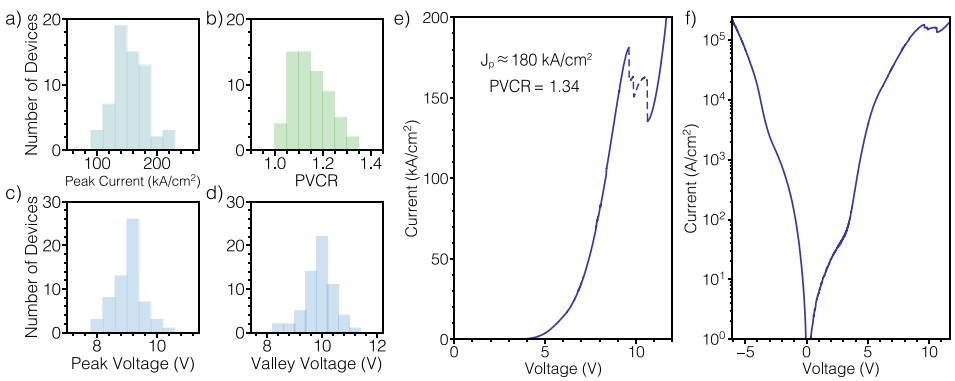

FIG. 2. Distribution of the (a) peak current density, (b) peak to valley current ratio (PVCR), (c) peak voltage, and (d) valley voltage measured in 62 devices across a single chip. (e) Room temperature current-voltage (*I-V*) characteristics of a RTD with a mesa area of $\sim 5 \times 5\ \mu m^2$. (f) Semilogarithmic plot showing the asymmetric *I-V* of the same device at room temperature.

DC voltage source and a spectrum analyzer, as schematically shown in the inset of Fig. 3(a). The DC characteristics of the resonant diode are displayed in Fig. 3(b). When the device is biased at 9.8 V, it oscillates, generating the power spectrum shown in Fig. 3(a). Under these conditions, the oscillator circuit provides an output power of ~3.0 μW into a 50 Ω load with a fundamental oscillation frequency of ~0.94 GHz. The oscillation frequency is limited by the time constant of the external circuit instead of the intrinsic tunneling time of the RTD. Moreover, the large impedance mismatch between the device and the 50 Ω load of the spectrum analyzer results in a limited microwave output power.

The maximum intrinsic frequency of oscillation f_{max} is estimated by calculating the resistive cutoff frequency of the small-signal equivalent circuit model for a RTD[38]

$$f_{max} = \frac{1}{2\pi C}\sqrt{\frac{-G_{max}}{R_s} - G_{max}^2}. \quad (1)$$

Here, G_{max} is the maximum NDC provided by the device, C is the RTD capacitance, and R_s is the series resistance.

To obtain G_{max}, a physics-based model[39] was used to fit the experimental I-V curve of our devices. Figure 3(b) shows the agreement between the measured and theoretical I-V characteristics which extend over the whole forward bias range. The theoretical expressions for the current components are given by

$$J_{RT}(V) = A\ln\left[\frac{1+e^{(B-C+n_1V)e/kT}}{1+e^{(B-C-n_1V)e/kT}}\right]\left[\frac{\pi}{2}+\tan^{-1}\left(\frac{C-n_1V}{D}\right)\right]$$

$$J_{TH}(V) = H\left(e^{n_2eV/kT}-1\right),$$

where J_{RT} is the resonant tunneling current and J_{TH} is the thermionic component.[39] The fitting parameters used for this particular device are as follows: $A = 4.76\times10^4$, $B = 3.6\times10^{-2}$, $C = 2.42\times10^{-1}$, $D = 1.08\times10^{-2}$, $n_1 = 2.43\times10^{-2}$, $H = 36.8$, and $n_2 = 1.89\times10^{-2}$.

From the RTD model, we obtain $G_{max} \approx -25$ mS. Meanwhile, the RTD capacitance can be calculated taking into account the device geometry and the depletion width x_d that forms in the collector region [see the bottom panel of Fig. 1(a)]. Using this approach, we estimate $C \approx 60$ fF, while the series resistance has been measured from the TLM structures, obtaining $R_s \approx 4$ Ω. Using Eq. (1), a maximum oscillation frequency of $f_{max} \approx 200$ GHz is calculated. This value is within the same order of magnitude as the oscillation frequencies obtained previously from GaAs/AlAs[36] and InGaAs/AlAs[32] RTDs.

Looking forward, RTDs with larger PVCRs and J_p will be required for fabricating high-power oscillators. From Fig. 3(b), we can see that the modest PVCR is a consequence of the large thermionic current, which grows exponentially with RTD bias. In this sense, decreasing the peak voltage can lead to devices with lower thermionic current levels and higher PVCRs, which could be achieved using thinner barriers. From our analytical model, it was determined that high-current GaN/AlN RTDs with $J_p \sim 1$ MA/cm^2 could be achieved using a symmetric double-barrier structure with a 2 nm (8 ML) quantum well sandwiched between 1.25 nm (5 ML) AlN tunneling barriers. Moreover, it is feasible to reduce the series resistance by ~10× with improved ohmic contacts and thinned substrates, thus obtaining a specific device resistance <10 Ω μm^2. In addition, further optimization of the doping and collector spacer should also result in a reduced device capacitance,[37] thus achieving oscillations with $f_{max} \sim 1$ THz. These results demonstrate that III-Nitride RTDs are promising candidates for the fabrication of THz electronic sources, significantly beyond the cutoff frequencies of III-Nitride HEMTs.[1–4]

To summarize, we have investigated III-Nitride RTDs which exhibit a record-high peak current density of ~220 kA/cm^2 at room temperature. When biased in the NDC region, self-oscillations are measured with a fundamental frequency of ~0.94 GHz, generating a microwave power of ~3.0 μW. The oscillation frequency and output power are limited by the biasing circuit and mismatched network, respectively. Furthermore, theoretical calculations show that oscillations up to 200 GHz could be generated by these devices using an adequate resonant circuit. Finally, an optimized device structure should be able to provide oscillations approaching 1 THz.

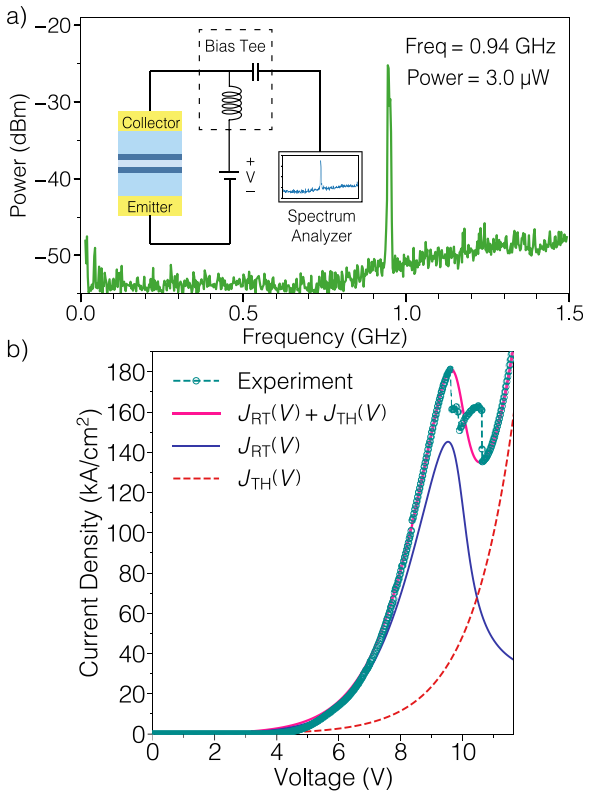

FIG. 3. (a) Power spectral density generated by the III-Nitride RTD oscillator. The inset shows the circuit schematic employed to measure self-oscillations using a spectrum analyzer. (b) Current-voltage characteristics measured in a device undergoing microwave self-oscillations. A physics-based model was employed to obtain the theoretical DC characteristics of the diode under non-oscillatory conditions.

The authors thankfully acknowledge the funding assistance from the Office of Naval Research under the DATE MURI Program (Contract: N00014-11-10721, Program Manager: Dr. Paul Maki) and from the National

Science Foundation under the NSF-DMREF Program (Contract: 1534303, Program Manager: Dr. John Schlueter).

[1]T. Suemitsu, IEICE Electron. Express **12**, 20152005 (2015).
[2]Y. Tang, K. Shinohara, D. Regan, A. Corrion, D. Brown, J. Wong, A. Schmitz, H. Fung, S. Kim, and M. Micovic, IEEE Electron Device Lett. **36**, 549 (2015).
[3]K. Shinohara, D. C. Regan, Y. Tang, A. L. Corrion, D. F. Brown, J. C. Wong, J. F. Robinson, H. H. Fung, A. Schmitz, T. C. Oh, S. J. Kim, P. S. Chen, R. G. Nagele, A. D. Margomenos, and M. Micovic, IEEE Trans. Electron Devices **60**, 2982 (2013).
[4]Y. Yue, Z. Hu, J. Guo, B. Sensale-Rodriguez, G. Li, R. Wang, F. Faria, B. Song, X. Gao, S. Guo, T. Kosel, G. Snider, P. Fay, D. Jena, and H. G. Xing, Jpn. J. Appl. Phys., Part 1 **52**, 08JN14 (2013).
[5]M. I. Dyakonov and M. S. Shur, IEEE Trans. Electron Devices **43**, 1640 (1996).
[6]M. Dyakonov and M. Shur, IEEE Trans. Electron Devices **43**, 380 (1996).
[7]B. Sensale-Rodriguez, L. Liu, P. Fay, D. Jena, and H. G. Xing, IEEE Trans. Terahertz Sci. Technol. **3**, 200 (2013).
[8]R. Tsu and L. Esaki, Appl. Phys. Lett. **22**, 562 (1973).
[9]L. L. Chang, L. Esaki, and R. Tsu, Appl. Phys. Lett. **24**, 593 (1974).
[10]M. Asada and S. Suzuki, J. Infrared, Millimeter, Terahertz Waves **37**, 1185 (2016).
[11]E. R. Brown, J. R. Söderström, C. D. Parker, L. J. Mahoney, K. M. Molvar, and T. C. McGill, Appl. Phys. Lett. **58**, 2291 (1991).
[12]S. Sakr, Y. Kotsar, M. Tchernycheva, E. Warde, N. Isac, E. Monroy, and F. H. Julien, Appl. Phys. Express **5**, 052203 (2012).
[13]J. Encomendero, F. Afroz Faria, S. M. Islam, V. Protasenko, S. Rouvimov, P. Fay, D. Jena, and H. G. Xing, preprint arXiv:1606.08100 [cond-mat.mes-hall] (2016).
[14]J. Encomendero, F. A. Faria, S. M. Islam, V. Protasenko, S. Rouvimov, B. Sensale-Rodriguez, P. Fay, D. Jena, and H. G. Xing, Phys. Rev. X **7**, 041017 (2017).
[15]T. A. Growden, D. F. Storm, W. Zhang, E. R. Brown, D. J. Meyer, P. Fakhimi, and P. R. Berger, Appl. Phys. Lett. **109**, 083504 (2016).
[16]D. Li, L. Tang, C. Edmunds, J. Shao, G. Gardner, M. J. Manfra, and O. Malis, Appl. Phys. Lett. **100**, 252105 (2012).
[17]D. Li, J. Shao, L. Tang, C. Edmunds, G. Gardner, M. J. Manfra, and O. Malis, Semicond. Sci. Technol. **28**, 074024 (2013).
[18]A. Grier, A. Valavanis, C. Edmunds, J. Shao, J. D. Cooper, G. Gardner, M. J. Manfra, O. Malis, D. Indjin, Z. Ikonić, and P. Harrison, J. Appl. Phys. **118**, 224308 (2015).
[19]H. Sugiyama, A. Teranishi, S. Suzuki, and M. Asada, Jpn. J. Appl. Phys., Part 1 **53**, 031202 (2014).
[20]T. Inata, S. Muto, Y. Nakata, T. Fujii, H. Ohnishi, and S. Hiyamizu, Jpn. J. Appl. Phys., Part 2 **25**, L983 (1986).
[21]R. Izumi, S. Suzuki, and M. Asada, in *42nd International Conference on Infrared, Millimeter, and Terahertz Waves (IRMMW-THz)* (2017), pp. 1–2.
[22]M. A. Belkin and F. Capasso, Phys. Scripta **90**, 118002 (2015).
[23]A. N. Baranov and R. Teissier, IEEE J. Select. Top. Quantum Electron. **21**, 85 (2015).
[24]R. Songmuang, G. Katsaros, E. Monroy, P. Spathis, C. Bougerol, M. Mongillo, and S. De Franceschi, Nano Lett. **10**, 3545 (2010).
[25]R. Dwiliński, R. Doradziński, J. Garczyński, L. Sierzputowski, A. Puchalski, Y. Kanbara, K. Yagi, H. Minakuchi, and H. Hayashi, J. Crystal Growth **310**, 3911 (2008).
[26]B. Ricco and M. Y. Azbel, Phys. Rev. B **29**, 1970 (1984).
[27]I. Tan, G. L. Snider, L. D. Chang, and E. L. Hu, J. Appl. Phys. **68**, 4071 (1990).
[28]M. O. Manasreh and G. L. McCoy, *Semiconductor Quantum Wells and Superlattices for Long-Wavelength Infrared Detectors* (Artech House Publishers, 1993).
[29]M. Tchernycheva, L. Nevou, L. Doyennette, F. H. Julien, E. Warde, F. Guillot, E. Monroy, E. Bellet-Amalric, T. Remmele, and M. Albrecht, Phys. Rev. B **73**, 125347 (2006).
[30]T. C. L. G. Sollner, P. E. Tannenwald, D. D. Peck, and W. D. Goodhue, Appl. Phys. Lett. **45**, 1319 (1984).
[31]L. Wang, J. M. L. Figueiredo, C. N. Ironside, and E. Wasige, IEEE Trans. Electron Devices **58**, 343 (2011).
[32]M. Feiginov, C. Sydlo, O. Cojocari, and P. Meissner, EPL (Europhys. Lett.) **97**, 58006 (2012).
[33]E. R. Brown, T. C. L. G. Sollner, W. D. Goodhue, B. J. Clifton, and P. E. Tannenwald, IEEE Trans. Electron Devices **33**, 1864 (1986).
[34]E. R. Brown, T. C. L. G. Sollner, W. D. Goodhue, and C. D. Parker, Appl. Phys. Lett. **50**, 83 (1987).
[35]E. R. Brown, W. D. Goodhue, and T. C. L. G. Sollner, J. Appl. Phys. **64**, 1519 (1988).
[36]E. R. Brown, T. C. L. G. Sollner, C. D. Parker, W. D. Goodhue, and C. L. Chen, Appl. Phys. Lett. **55**, 1777 (1989).
[37]H. Kanaya, R. Sogabe, T. Maekawa, S. Suzuki, and M. Asada, J. Infrared, Millimeter, Terahertz Waves **35**, 425 (2014).
[38]T. C. L. G. Sollner, E. R. Brown, W. D. Goodhue, and H. Q. Le, Appl. Phys. Lett. **50**, 332 (1987).
[39]J. N. Schulman, H. J. D. L. Santos, and D. H. Chow, IEEE Electron Device Lett. **17**, 220 (1996).